

Article

New Insights into Coloration Mechanism in Violet-Red Pyrope-Almandine

Puyue Yang¹ and Ying Guo^{2,*} 

¹ Department of Gemstone and Materials Technology, Sichuan University of Culture and Arts, Mianyang 621000, China; 2009180020@email.cugb.edu.cn

² School of Gemmology, China University of Geosciences, Beijing 100083, China

* Correspondence: guoying@cugb.edu.cn

Abstract: The most common type of garnet is pyrope-almandine, whose color varies from red to violet. In this study, 36 faceted gem-quality samples are used for electron microprobe, infrared spectrum, and UV-Visible spectrum test to find the coloration mechanism and spectroscopic characters in red-violet pyrope-almandine. The gradually increasing content of Mg²⁺ at the X position in the lattice is connected to the variation in the infrared spectrum. The wavenumber increases with the decrease of cationic radius, which makes the distance between C and D bands further. The color mechanism is mainly affected by Fe²⁺, and Mn²⁺. We discuss the change in colors with the assumption of a certain MnO content. When it is above or below the standard of 1 wt%, the absorption intensity of the UV-Visible spectrum is completely different in the purple zone, which determines the color to be red or violet. Therefore, the effect of Mn²⁺ and Fe²⁺ should be combined instead of being considered respectively. The results show that the MnO content can be quickly inferred by the light purple/fancy purple color. To avoid harming the value, this new insight makes it possible to quickly classify the gem quality in mining as well as in the market.

Keywords: garnet; spectroscopic analysis; color cause; determining species



Citation: Yang, P.; Guo, Y. New Insights into Coloration Mechanism in Violet-Red Pyrope-Almandine. *Crystals* **2022**, *12*, 379. <https://doi.org/10.3390/cryst12030379>

Academic Editors: Taijin Lu, Fei Liu, Tingting Gu and Francesco Capitelli

Received: 26 January 2022

Accepted: 8 March 2022

Published: 11 March 2022

Publisher's Note: MDPI stays neutral with regard to jurisdictional claims in published maps and institutional affiliations.



Copyright: © 2022 by the authors. Licensee MDPI, Basel, Switzerland. This article is an open access article distributed under the terms and conditions of the Creative Commons Attribution (CC BY) license (<https://creativecommons.org/licenses/by/4.0/>).

1. Introduction

Garnet is a widespread mineral, existing on the crust and upper mantle with the chemical formula X₃Y₂(SiO₄)₃ [1]. As an island silicate, the isolated [SiO₄] tetrahedra in garnet forms the crystalline base of the crystal, combining with [YO₆] octahedron and [XO₈] dodecahedron repeatedly to make up the structure (Figure 1) [2]. The shared corners of both [YO₆] octahedrons and isolated silicon-oxygen tetrahedrons make it workable to form a dodecahedron vacuum between them. This vacuum is centered on X²⁺, shaped as a distorted cubic [3]. Most of the ions can be substituted by similar particles, which is due to the fact that garnet is a complete isomorphous series [4].

As a quick and non-destructive testing method, IR spectroscopy is indispensable for researchers to figure out which functional groups exist in the minerals and how they affect every aspect [5]. The infrared (IR) spectrum can be used as proof to infer the proportion of each garnet end-member through the different functional groups' activities [6].

Referring to the coloration mechanism, other researchers have proposed diverse hypotheses which can be summarized under three basic theories: crystal field theory, molecular orbital theory, and band theory. The key of these theories is similar in that they propose that electron motion causes the selective absorption of light which results in different colors, and that these colors vary depending on the range of the electrons' moving space. Based on the complex isomorphism, the color as well as other characters vary from kind to kind. Due to the component of the transition metal compounds formed from the first transition elements (V, Cr, Mn, Fe), garnets have a rich palette of colors. According to the crystal structure of garnets, the cause of coloration belongs to crystal

field theory. In nature, as a complete isomorphic series, garnets are always mined as a solid solution [7,8]. Therefore, UV-Visible spectroscopy is an ideal method to measure their absorption spectrum, which is connected to the characteristic spectrum generated by electron energy absorption or release under the action of electromagnetic radiation.

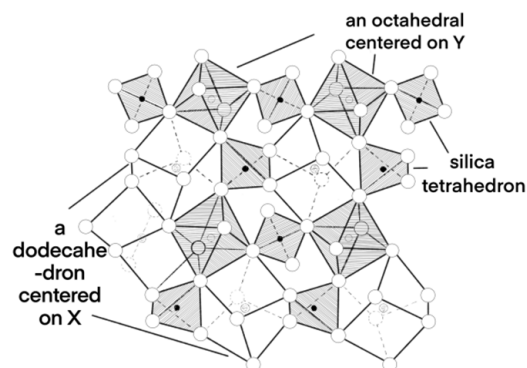


Figure 1. The crystal structure of garnet, modified from Novak et al. [2].

The samples, termed pyrope-almandine, belong to the pyralspite series. In this series, Al^{3+} occupies the Y position, and the X position is principally occupied by Fe^{2+} and Mg^{2+} . However, sometimes a small amount of Mn^{2+} can substitute the Fe^{2+} and Mg^{2+} [9]. The color of minerals depends on the color of the oxide of the elements they have [10]. Mg is insignificant for coloration as a non-transition element, which means the purple-red color is the result of Fe^{2+} and Mn^{2+} [11,12]. Besides, some trace elements can't be ignored as they are infrequent in proportion to other elements but have a disproportionately significant influence, such as V^{3+} and Cr^{3+} . However, this part of the research requires further test [13]. The color, as a comprehensive result of chromophores, makes it difficult to separate the influence of a single element, respectively, during others' research [14].

The Malaya garnet from Bekily, Madagascar has a similar pink-pinkish orange color while the samples do not show enough similarity in chemical composition, especially in the Mn component [14]. The authors elaborated that the color of the Malaya garnet is caused by its high manganese content, which causes intense absorption in the purple zone. Compared with the rare Malaya garnet, the red-violet garnet (pyrope-almandine) without significant manganese is the more common series [15]. However, few papers discussed the coloration mechanism or briefly mentioned it. Moreover, it is strange that some iron-rich pyrope shows completely different colors. To avoid harming the values, this new insight makes it possible to quickly classify the gem quality in mining as well as the market. Secondly, as the most precious one in this series, the fancy purple garnets can easily be found in the mineral deposit with a certain condition of Mn and Fe.

In this paper, to figure out the relationship between red-violet color and relative higher ferrum composition, different colors of pyrope-almandine have been chosen to be tested by electron microprobe. Every oxide content has been analyzed by the Cation method. In addition, we investigated the influence of ions on the IR spectrum and UV-Visible spectrum, which are connected to body color directly and chemical composition indirectly.

2. Materials and Methods

2.1. Samples Description

There are 59 samples of pyrope-almandine, which differ in hue, chroma, and lightness (Figure 2). We collected the samples in order to cover all of the colors of pyrope-almandine. The range of weight varies from 0.94 to 2.78 carat, and the shape is between 4 and 8 mm. All samples are cut and polished with various cuts, including emerald, oval, heart, pear, round, and rectangle. All of them are good in transparency, due to the high clarity is a basic guarantee of test accuracy. The standard gemological characteristics of samples are listed

in Table 1. The purple ones are numbered as P1–P27, and the red ones are numbered as R1–R32, the hue is determined by the color measurement instrument below.

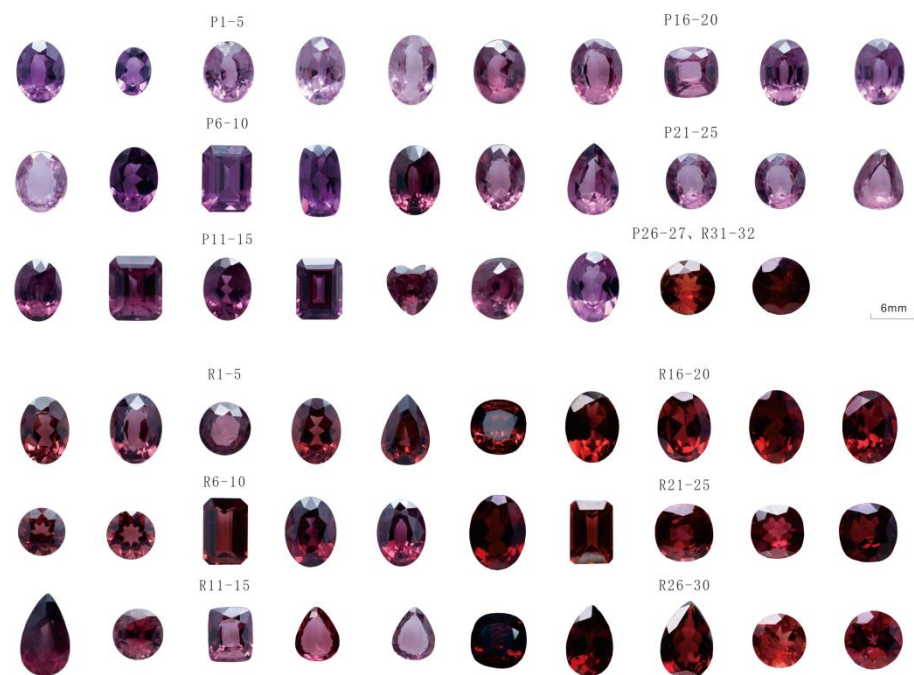


Figure 2. Violet to red pyrope-almandine which differ from the hue, chroma, and lightness.

Table 1. Standard gemological characteristics of the samples.

Samples Number	Weight (g)	SG	RI	Color
P1	0.332	3.851	1.763	Purple
P2	0.267	3.874	1.764	Purple
P3	0.239	3.789	1.743	Light purple
P4	0.243	3.751	1.745	Light purple
P5	0.187	3.809	1.747	Light purple
P7	0.288	3.914	1.770	Deep purple
P11	0.389	3.875	1.756	Deep reddish purple
P15	0.389	3.821	1.755	Deep reddish purple
P20	0.417	3.745	1.745	Reddish purple
R1	0.237	3.839	1.756	Purplish red
R3	0.235	3.830	1.761	Purplish red
R10	0.338	3.867	1.767	Deep purplish red
R12	0.371	3.782	1.752	Deep purplish red
R15	0.310	3.771	1.749	Light purplish red
R16	0.277	3.788	1.744	Red
R26	0.235	3.986	1.773	Deep red

2.2. Electron Microprobe

The chemical compositions of studied pyrope-almandine are determined by the JXA8100 electron microprobe, produced in Tokyo, Japan. The samples are tested in the Beijing Institute of Geology of Nuclear Industry. According to their colors, 36 samples have been chosen for investigation which has a significant difference in hue. The samples are fixed on the blue tack to ensure the surface which is sprayed with a layer of toner is perpendicular to the microprobe. The operating conditions are as follows: 20 kV accelerating voltage; 1×10^{-8} A beam current and 40° emergence angle. The analysis method is spectral analysis, and the correction method is ZAF. Every sample has been tested once as the investigated garnets are cubic system gems that are constant in all directions. The following

standards were used: jadeite (Si and Al), forsterite (Mg), wollastonite (Ca), hematite (Fe), rutile (Ti), MnO (Mn), and Cr₂O₃ (Cr) have been used as standards. The structural formula of garnet was calculated by the program WinTcac created by Locock, A.J. (2008). The contents of FeO and Fe₂O₃ were acquired by stoichiometry, based on $X + Y + Si = 8 \text{ apfu}$, $O = 12 \text{ apfu}$ [16].

2.3. UV-Visible Spectroscopy

In different crystal structures, different types of electronics show various activity characters, resulting in the minerals showing different reactions of electromagnetic radiation. The selective absorption of the studied pyrope-almandine is determined by using Japan Shimadzu UV-3600 UV-Visible spectroscopy, produced in Canby, OR, USA. The samples are tested in the Gemological Experimental Teaching Center of China University of Geosciences (Beijing). The test wavelength range is 300–900 nm, the measurement method is reflectivity, time constant: 1 s, light source conversion wavelength: 300 nm, detector conversion wavelength: 900 nm, grating conversion wavelength: 900 nm, beam mode: double beam. Since the equation for absorbance (A) is: $A = \text{extinction coefficient} \times \text{concentration of absorbent} \times \text{thickness}$, the spectrum has been modified by the multiplication of the appropriate factor [17].

2.4. IR Spectroscopy

The test site of Infrared Spectroscopy is the Gemological Experimental Teaching Center of China University of Geosciences (Beijing, China), and the instrument we used in the experiment is BRUKER Tensor 27 (Bremen, German), a German Fourier transform infrared spectrometer.

The test conditions are as follows: the scanning range was 400–1500 cm^{-1} , the scanning time of the sample and Beijing is 8 SCANS, and the scanning speed is 7.5 KHz. Power supply 85–265 V, power supply frequency 47–65 Hz, temperature 18–35 °C, humidity < 70%, resolution 4 cm^{-1} , grating setting 6 mm, sample scanning times 50–100, test mode is reflection mode. Spectra were recorded in the range of 400–1250 cm^{-1} . Based on the consensus that garnet is isotropic, randomly oriented crystals are tested as the properties are constant in all directions.

2.5. Color Measurement Instrument

The instrument we used to measure the color is LiuLalbs MDIS-8 multifunctional double integrating sphere spectrometer, produced in China. A specially designed double integrating sphere optical system provides optimal illumination and geometric conditions for measuring spectral reflection and color of faceted colored gems and diamonds in a controlled environment. To ensure the accuracy of spectral and color measurements, the spectrometer adopts a novel three-step calibration method. The trained neural network input shape, size and refractive index, and output numerical parameters to control the spectrometer to accurately measure the spectral reflectance of the inscribed gem, and output strategy parameters for the fuzzy logic algorithm to determine the true color level. This instrument is more applicable for faceted gems as it can modify the coloration data by the size and cut of the samples that you input in. To be more precise, each sample has been tested three times and the average is taken as the result.

3. Results

3.1. Electron Microprobe

Through the calculation, the proportions of the oxides and end-member components are listed in Table 2. Assuming that the proportions of the three end-member components of pyrope series add up to 100 percent, the group can be determined and the results are shown in Figure 3. All of the samples are pyrope-almandine without significant content of spessartine. The red ones have more proportion of almandine than purple ones, showing the importance of high-level ferrum to red colors.

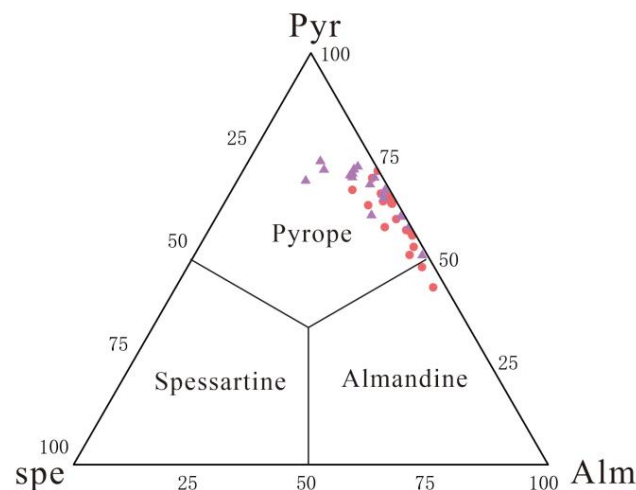


Figure 3. Pyralspite series classification based on the cation proportions of the X position. The red dots represent the red samples. The purple triangles show the characters of purple ones.

The range of chemical content proportions are as below (wt%): FeO = 11.48–21.99, MgO = 9.76–18.59, MnO = 0.11–3.52, Cr₂O₃ = 0.00–0.08 (red samples); FeO = 6.77–21.19, MgO = 12.56–19.82, MnO = 0.17–7.70, Cr₂O₃ = 0.00–0.18 (purple samples). Part of the data is listed in Table 2 as necessary. When the content of pyrope end member is higher than 75%, no red samples be found in the high manganese and low ferrum region, but all purple. The samples with relatively high manganese in pyrope-almandine display all red.

Table 2. Representative chemical compositions of red-purple pyrope-almandine tested by electron microprobe (wt%).

Sample Number	P1	P2	P3	P4	P5	P7	P11	P15	P20	R1	R3	R10	R12	R15	R16	R26
Oxide/(wt%)																
SiO ₂	39.88	40.39	41.20	41.88	40.99	39.33	40.34	40.27	41.49	40.66	40.07	40.54	41.43	41.05	41.85	39.46
TiO ₂	0.00	0.00	0.03	0.04	0.00	0.02	0.04	0.03	0.00	0.04	0.08	0.07	0.04	0.06	0.03	0.00
Al ₂ O ₃	23.17	23.15	23.51	24.12	23.27	22.58	23.29	22.91	23.08	22.98	23.38	22.68	23.09	23.07	23.67	22.18
Cr ₂ O ₃	0.00	0.02	0.13	0.10	0.08	0.00	0.05	0.03	0.03	0.03	0.04	0.07	0.04	0.08	0.01	0.00
FeO	18.39	20.10	7.69	6.77	8.24	21.19	15.34	14.25	11.80	15.49	17.16	20.38	14.09	11.48	13.44	21.99
MnO	0.47	0.17	5.29	7.70	5.37	0.49	1.07	3.01	1.85	0.45	2.58	1.66	1.10	3.52	0.11	1.07
MgO	15.98	15.58	19.82	18.14	19.08	12.56	16.85	14.90	19.41	15.98	15.10	12.82	18.59	16.88	18.91	9.76
CaO	0.97	0.70	1.99	1.46	1.61	1.19	1.36	2.61	1.35	3.86	1.63	1.17	1.71	2.28	0.96	3.57
Tatol	98.86	100.11	99.66	100.21	98.64	97.36	98.34	98.01	99.01	99.49	100.04	99.39	100.09	98.42	98.98	98.03
Atomic proportions based on X + Y + Si = 8 apfu																
Si	2.97	2.98	2.96	3.00	2.98	3.01	2.98	3.01	3.00	2.99	2.96	3.04	2.99	3.02	3.02	3.04
Ti	0.00	0.00	0.00	0.00	0.00	0.00	0.00	0.00	0.00	0.00	0.00	0.00	0.00	0.00	0.00	0.00
Al	2.03	2.01	1.99	2.04	2.00	2.04	2.03	2.02	1.97	1.99	2.04	2.00	1.96	2.00	2.02	2.01
Cr	0.00	0.00	0.01	0.01	0.01	0.00	0.00	0.00	0.00	0.00	0.00	0.00	0.00	0.01	0.00	0.00
Fe ³⁺	0.00	0.00	0.03	0.00	0.01	0.00	0.00	0.00	0.03	0.02	0.00	0.00	0.04	0.00	0.00	0.00
Fe ²⁺	1.14	1.24	0.44	0.41	0.49	1.36	0.95	0.89	0.69	0.93	1.06	1.28	0.81	0.71	0.81	1.42
Mn	0.03	0.01	0.32	0.47	0.33	0.03	0.07	0.19	0.11	0.03	0.16	0.11	0.07	0.22	0.01	0.07
Mg	1.77	1.71	2.12	1.94	2.07	1.43	1.86	1.66	2.09	1.75	1.66	1.43	2.00	1.85	2.04	1.12
Ca	0.08	0.06	0.15	0.11	0.13	0.10	0.11	0.21	0.11	0.30	0.13	0.09	0.13	0.18	0.07	0.30

3.2. UV-Visible Spectrum

The experimental results of UV-Visible spectrum show that the peaks of UV-Visible absorption spectra are almost the same, but the intensity of each peak changes as iron concentration differs. The assignment of the bands at 503, 610, 687 nm to Fe²⁺, and at 413 nm to Mn²⁺ [15]. However, the absorption character of garnets is confused in the overlap. Due to the lack of the pure spessartine in 1960s to 1970s, the absorption bands of manganese and iron can't be separated, respectively, as they are at approximately the same position, which is proved in the iron-poor spessartine from Namibia and Nigeria. We agree

with the assessment of the updated literature on this topic [14]. However, the absorption at 460 nm shows a clear positive correlation to the content of Fe^{2+} , which is more accurate to be assigned to Fe^{2+} . The content of Fe^{3+} is almost nonexistent, so it cannot be ensured if there has weak absorption of Fe^{3+} at 424 nm. Otherwise, the intensity of absorption at 572 nm shows no definite changes with variable content of Fe^{2+} . It can be suggested that there are other elements which affect the intensity [18]. The assignments of the absorption peaks are listed in Table 3.

Table 3. Assignment of absorption maxima observed in pyrope-almandine. The assignment of the bands is signed by tick.

Absorption Peaks	Fe^{2+}	Mn^{2+}	$\text{V}^{3+}/\text{Cr}^{3+}$
410 nm	-	✓	-
424 nm	-	✓	-
460 nm	✓	-	-
503 nm	✓	-	-
523 nm	✓	✓	-
572 nm	✓	-	✓
610 nm	✓	-	-
687 nm	✓	-	-

The absorption peaks at 460, 610, and 687 nm disappear in the poor-iron pyrope, and the intensity gradually raises with the rise of ferrum and loss of manganese. The purple sample has strong absorption in the end of the purple region with an absorbed yellow-green region, while there is a transmission area in orange-red zone [19]. Four characteristic samples with the ratio of $\text{FeO}:\text{MnO}$ from low to high are selected to be illustrated in Figure 4.

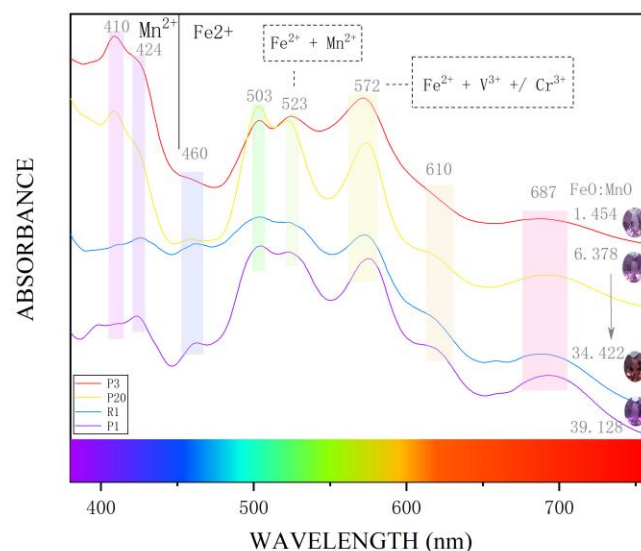


Figure 4. Absorption spectra of four faceted pyrope-almandine shows systematic variations according to their iron and manganese contents. The color varies from light violet (at lower $\text{FeO}:\text{MnO}$ ratios) to purplish red (at higher $\text{FeO}:\text{MnO}$ ratios), and alters to fancy violet ultimately (at highest $\text{FeO}:\text{MnO}$ ratios). The sample P3 and P20 are similar with both relatively medium iron contents, but the rest samples show similar absorption features with different color.

The spectra of the samples with different $\text{FeO}:\text{MnO}$ ratios shows the high similarity of the absorption in the yellow and green zones. As the $\text{FeO}:\text{MnO}$ ratio increases, the sample has more Fe and less Mn, leading to the absorption of the orange-red region becoming stronger, while the absorption of the purple region becomes weaker, increasing the absorption of the blue region. On the contrary, when the ratio decreases, the absorption

in the purple region is enhanced and the absorption in the orange-red and blue region gets weaker. This phenomenon will provide strong evidence to explore the relationship between color and chemical composition.

3.3. IR Spectroscopy

The vibration peak of 400–1000 cm^{-1} belongs to the internal vibrations of the SiO_4 tetrahedra. The vibration peak of 800–1000 cm^{-1} represents asymmetric Si-O stretching vibrations (V3), the vibration peak of 500–800 cm^{-1} represents asymmetric bending vibrations (V4), and symmetric bending vibrations V2 is in the range of 400–500 cm^{-1} [20]. The absorption peaks with a wave number less than 500 cm^{-1} are related to the external vibrations, among which H and I absorption peaks are related to trivalent cations. The infrared spectral images of the samples have the same general trend, which accords with the characteristic spectrum of pyrope-almandine [20,21].

A and B peaks (993–999 cm^{-1}) form the A wide absorption band; the C peak is in 904–914 cm^{-1} , the E peak is missing (635 cm^{-1}) in the pyrope-rich compositions, the F peak is near 586 cm^{-1} , and D (875–881 cm^{-1}) and G (534–536 cm^{-1}) appear in the form of acromion. H and I exist in the vicinity of 490 cm^{-1} and 460 cm^{-1} , respectively. The deviation of peak position is related to the chemical composition of garnet, so four samples with regular changes in chemical composition are selected for comparison of IR spectra (Figure 5).

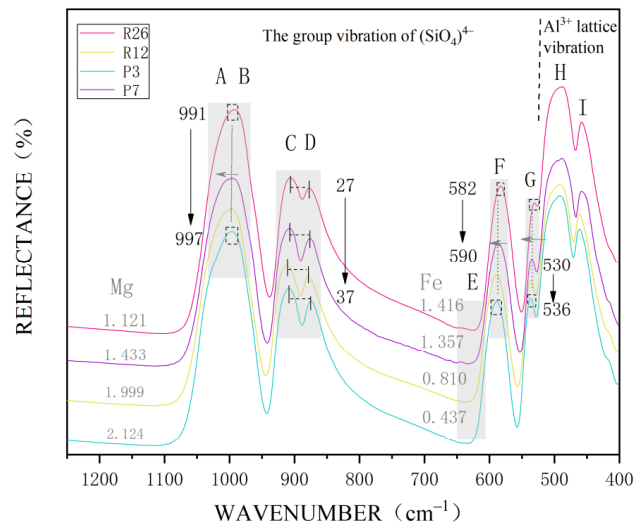


















Figure 5. IR absorption spectra of four faceted pyrope-almandine shows systematic variations according to their iron and manganese contents. The wave number of A–G bands alter to be larger with the increase of manganese. The E band doesn't occur due to the pyrope-rich composition.

3.4. Color Quantization

Identifying the colors is a very delicate operation; the color measurement instrument is more suitable for quantization than unaided eyes. The colors are always described with three basic parameters, namely hue, chrome, and lightness. The color quantization for investigated samples is listed in Table 4. The CIE 1976 $L^*a^*b^*$ Uniform color space is the recommended standard for color characterization due to its accuracy and wide applicability. For the sake of research, the $L^*a^*b^*$ data are transformed to L^* , C^* , h_o [22].

Table 4. Color quantization of investigated pyrope-almandine, and the color simulation which is transformed by COLORTELL website. (<http://www.colortell.com>, accessed on 6 October 2021).

Sample Num.	L*	C*	h_0	Color Simulation
P1	23.82	45.18	334.48	
P2	28.30	52.63	331.91	
P3	24.82	36.87	350.39	
P4	55.54	34.97	352.38	
P5	38.77	21.38	355.79	
P7	23.17	44.10	338.84	
P11	28.16	43.16	355.11	
P15	17.81	33.28	359.15	
P20	36.94	40.34	345.08	
R1	23.65	35.42	13.06	
R3	13.24	25.00	6.14	
R10	16.63	36.29	4.42	
R12	30.18	49.17	1.88	
R15	26.79	19.43	0.11	
R16	33.26	51.86	31.17	
R26	10.29	37.31	6.86	

4. Discussion

4.1. Chemical Compositions Variation and the Influence on Color

To explore the relationship between garnet color and composition, it is necessary to set a standard to describe changes of color accurately.

Through the UV-Vis spectrum, the small amount of Mn^{2+} ($MnO > 1$ wt%) in the garnet can cause strong absorption in the purple zone, resulting in more red light to reserve. Otherwise, when the content of MnO decreases below 1 wt%, the absorption intensity in the purple zone is too low to absorb enough purple light. Although the content of MnO increases again to 7–10 wt%, the absorption intensity shows no obvious change in the purple zone, indicating that when Mn^{2+} content increased to a certain concentration (3 wt%), the continued increase has no significant effect on color. Under the condition of $MnO > 1$ wt%, the purple light is almost completely absorbed, resulting in few residual purple lights. This finding is also proved by color quantization data. The MnO content of P1 and P2, which have a hue angle of purple, was lower than 1 wt%, ranging from 0.17 to 0.47 wt%.

Regardless of how much Fe^{2+} content the sample has, the yellow-green region is absorbed in a stable way, while the absorption intensity of the red-orange region depends on the ratio of $FeO:MnO$. When the ratio is low to 1.454, the absorption of the red and blue region almost disappears. Based on the purple area being strongly absorbed in high-Mn pyrope, the left red lights mix the blue lights, making the garnet shows light purple. For instance, the samples P3, and P20 have a high lightness (24.82, 36.94) and purple hue (which determined by the hue angle). On the contrary, when the MnO content is lower than 1 wt% to absorb enough purple light, the absorption in the orange-red areas is strong, thus the residual purple area makes the color “pure” in purple tone without any other color light left. This type may have the fancy purple color, which is proved by the body color of P1, and P2, with the lowest hue angle as 334.48° and 331.91° .

When it comes to the samples with middle content of MnO and FeO , the color depends on the absorption intensity in red and purple zones, combined with the absorption characters of the two typical kinds above. If the red lights are absorbed more, the garnet displays purple color and vice versa. As the trace elements Fe^{3+} or V^{3+} and Cr^{3+} can contribute to the color, it requires further tests to investigate the effect on color [12,23].

4.2. Four Types of Pyrope-Almandine

Through the chemical compositions, the samples are separated into four types (Figure 6) and summarized in Table 5.

- I. Medium Fe, High Mn (FeO \approx 6–11 wt%; MnO \approx 3–8 wt%);
- II. Medium-High Fe, Low Mn (FeO \approx 11–23 wt%; MnO \approx 1–3 wt%);
- III. Medium Fe, Extremely Low Mn (FeO \approx 13–18 wt%; MnO \approx 0–1 wt%);
- IV. High Fe, Extremely Low Mn (FeO \approx 18–21 wt%; MnO \approx 0–1 wt%)

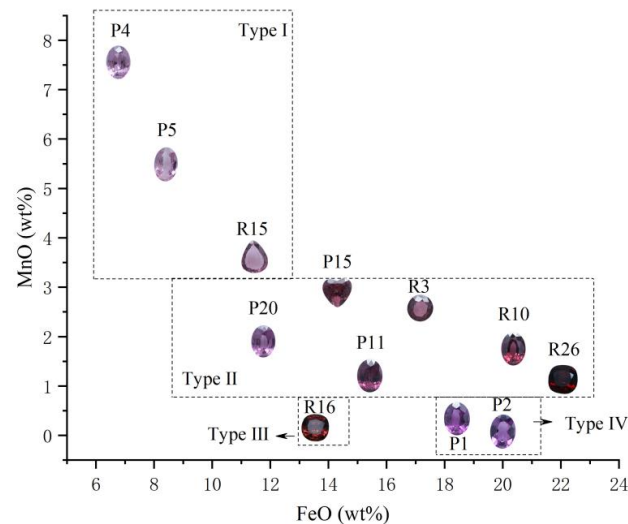


Figure 6. The color of pyrope-almandine is related to their chemical composition. The trend of color is comprehensive due to the complex action mode of Mn^{2+} . There are typical 12 samples of both color and chemical composition that illustrate the color cause clearly.

Table 5. The absorption characters, chemical contents, and color causes of four types garnet which result in the trend of color variation.

Type	I	II	III	IV
Color	Light purple	Purplish red-red	Red	Purple-fancy purple
Lightness range	26.79–55.54	10.29–36.94	33.26	23.82–28.30
Chrome range	19.43–34.97	25.00–43.16	51.86	45.78–52.63
Hue range	352.38–0.11	345.08–6.86	31.17	331.91–334.48
Dominated ion	Mn^{2+}	Mn^{2+}	Mn^{2+}/Fe^{2+}	Fe^{2+}
Absorption in purple region	Strong absorption	Strong absorption	Weak absorption	Weak absorption
Absorption in blue region	Weak absorption	Increase	Increase	Strong absorption
Absorption in yellow-green region	Strong absorption	Strong absorption	Strong absorption	Strong absorption
Absorption in orange-red region	Weak absorption	Increase	Increase	Strong absorption
Content of Mn^{2+}	high	Low	Extremely low	Extremely low
Content of Fe^{2+}	Medium	Medium-High	Medium	High
Color cause	Red + blue \rightarrow light purple	Left the red lights	Depending on which light has more left, red or purple	Absorb almost all color light except purple

4.3. IR Spectrum and the Chemical Composition

The wave numbers of A–G bands are negatively correlated with the cell parameter a_0 , which depends on the cationic size of X^{2+} and Y^{3+} . The wave number increases with the decrease of cationic radius. Since the ionic radii of ferrum and manganese ions are similar and larger than that of magnesium ions, the increase of magnesium content leads to the increase of band wave number [24]. In particular, the ratio of almandine in sample R26 is around 50%. According to this, when A, B peaks $> 991\text{ cm}^{-1}$, F peak $> 582\text{ cm}^{-1}$, G peak $> 530\text{ cm}^{-1}$, the garnet can be classified as pyrope.

The distance between C and D bands is related to the radius of the cation X^{2+} in the center of the dodecahedron [25]. In the structure, the silicon-oxygen tetrahedron is connected to the X^{2+} dodecahedron with an edge, and the shorter the distance between X^{2+} ion and Si^{4+} ion is, the stronger the coupling of them is. Therefore, a smaller A^{2+} radius will larger the distance between C and D bands. When the distance is longer than 27, the garnet is supposed to be a pyrope [26,27].

5. Conclusions

From the IR spectrum, we firstly determined the boundary between pyrope and almandine. When the distance between C, D bands > 27 and A, B peaks $> 991\text{ cm}^{-1}$, F peak $> 582\text{ cm}^{-1}$, G peak $> 530\text{ cm}^{-1}$ reveal the end-member of pyrope. Moreover, the Mn^{2+} content is essential to investigate the color of pyrope-almandine. Two typical types of samples display the relationship between color and chemical composition. One is a light purple sample which has a $\text{MnO} > 3\text{ wt\%}$ and extremely low level of FeO . In contrast, the fancy violet samples with the extremely pure violet hue show the characters of lowest content of $\text{MnO} < 1\text{ wt\%}$. However, these samples have a large amount of FeO .

The effect of Mn^{2+} is decided by the MnO proportion. The composition of MnO above 1 wt\% leads to strong absorption in the purple zone, resulting in stronger red-orange colors. When it is below the boundary, high-almandine pyrope turns to pure purple with relatively strong absorption in all zones except the purple zone. The result represents the feasibility for people to infer the chemical composition with naked eyes.

Author Contributions: Formal analysis, P.Y.; investigation, P.Y.; methodology, P.Y.; supervision, P.Y.; writing—original draft, P.Y.; writing—review and editing, Y.G. All authors have read and agreed to the published version of the manuscript.

Funding: This research received no external funding.

Data Availability Statement: All data we have mentioned are available in the article.

Conflicts of Interest: The authors declare no conflict of interest.

References

1. Sibi, N.; Subodh, G. Structural and Microstructural Correlations of Physical Properties in Natural Almandine-Pyrope Solid Solution: $\text{Al}_{70}\text{Py}_{29}$. *J. Electron. Mater.* **2017**, *46*, 6947–6956. [[CrossRef](#)]
2. Novak, G.A.; Gibbs, G.V. The Crystal Chemistry of the Silicate Garnets. *Am. Mineral.* **1971**, *56*, 791–825.
3. Geiger, C.A. A tale of two garnets: The role of solid solution in the development toward a modern mineralogy. *Am. Mineral.* **2016**, *101*, 1735–1749. [[CrossRef](#)]
4. Akizuki, M. Growth structure and crystal symmetry of grossular garnets from the Jeffrey Mine, Asbestos, Quebec, Canada. *Am. Mineral.* **1989**, *74*, 859–864.
5. Tarte, P.; Deliens, M. Correlations between the infrared spectrum and the composition of garnets in the pyrope-almandine-spessartine series. *Contrib. Mineral. Petrol.* **1973**, *40*, 25–37. [[CrossRef](#)]
6. Adamo, I.; Pavese, A.; Prospero, L.; Diella, V.; Ajò, D. Gem-quality garnets: Correlations between gemmological properties, chemical composition and infrared spectroscopy. *J. Gemmol.* **2007**, *30*, 307–319. [[CrossRef](#)]
7. Hoover, D.B. Determining Garnet Composition from Magnetic Susceptibility and Other Properties. *Gems Gemol.* **2011**, *47*, 272–275. [[CrossRef](#)]
8. Runciman, W.A.; Marc, M. The magnetic circular dichroism of pyrope-almandine garnets. *Am. Mineral.* **1975**, *60*, 1122–1124.
9. Manning, P.G. The optical absorption spectra of the garnets almandine-pyrope, pyrope and spessartine and some structural interpretations of mineralogical significance. *Can. Mineral.* **1967**, *9*, 237–251.
10. Yu, X.Y.; Long, Z.Y.; Zhang, Y.; Qin, L.J.; Zhang, C.; Xie, Z.R.; Wu, Y.R.; Yan, Y.; Wu, M.K.; Wan, J.X. Overview of Gemstone Resources in China. *Crystals* **2021**, *11*, 1189. [[CrossRef](#)]
11. Manson, D.V.; Stockton, C.M. Pyrope-spessartine garnets with unusual color behavior. *Gems Gemol.* **1984**, *20*, 200–207. [[CrossRef](#)]
12. Krzemnicki, M.S.; Hänni, H.A.; Reusser, E. Colour-change garnets from Madagascar: Comparison of colorimetric with chemical data. *J. Gemmol.* **2001**, *27*, 200–207. [[CrossRef](#)]
13. Venkateswarulu, P.; Rao, K.S.; Kasipathi, C.; Ramakrishna, Y. Multielemental analyses of isomorphous Indian garnet gemstones by XRD and external PIXE techniques. *Appl. Radiat. Isot.* **2012**, *70*, 2746–2754. [[CrossRef](#)] [[PubMed](#)]
14. Schmetzer, K.; Hainschwang, T.; Kiefert, L.; Bernhardt, H.J. Pink to Pinkish Orange Malaya Garnets from Bekily, Madagascar. *Gems Gemol.* **2001**, *37*, 296–308. [[CrossRef](#)]
15. Moore, R.K.; White, W.B. Electronic spectra of transition metal ions in silicate garnets. *Can. Mineral.* **1972**, *11*, 791–811.
16. Locock, A.J. An Excel spreadsheet to recast analyses of garnet into end-member components, and a synopsis of the crystal chemistry of natural silicate garnets. *Comput. Geosci.* **2008**, *34*, 1769–1780. [[CrossRef](#)]
17. Merkel, P.B.; Breeding, C.M. Spectral differentiation between copper and iron colorants in gem tourmalines. *Gems Gemol.* **2009**, *45*, 112–119. [[CrossRef](#)]
18. Krambrock, K.; Guimarães, F.S.; Pinheiro, M.V.B.; Paniago, R.; Righi, A.; Persiano, A.I.C.; Karfunkel, J.; Hoover, D.B. Purplish-red almandine garnets with alexandrite-like effect: Causes of colors and color-enhancing treatments. *Phys. Chem. Miner.* **2013**, *40*, 555–562. [[CrossRef](#)]

19. Eeckhout, S.G.; Castañeda, C.; Ferreira, A.C.M.; Sabioni, A.C.S.; Grave, E.D.; Vasconcelos, D.C.L. Spectroscopic studies of spessartine from Brazilian pegmatites. *Am. Mineral.* **2002**, *87*, 1297–1306. [[CrossRef](#)]
20. Geiger, C.A. A powder infrared spectroscopic investigation of garnet binaries in the system $Mg_3Al_2Si_3O_{12}$ - $Fe_3Al_2Si_3O_{12}$ - $Mn_3Al_2Si_3O_{12}$ - $Ca_3Al_2Si_3O_{12}$. *Eur. J. Mineral.* **1998**, *3*, 407–422. [[CrossRef](#)]
21. Hofmeister, A.M.; Chopelas, A. Vibrational spectroscopy of end-member silicate garnets. *Phys. Chem. Miner.* **1990**, *17*, 503–526. [[CrossRef](#)]
22. Sun, Z.Y.; Palke, A.C.; Renfro, N. Vanadium and Chromium-bearing pink pyrope garnet: Characterization and quantitative colorimetric analysis. *Gems Gemol.* **2015**, *51*, 348–369. [[CrossRef](#)]
23. Carstens, H. The red-green change in chromium-bearing garnets. *Contrib. Mineral. Petrol.* **1973**, *41*, 273–276. [[CrossRef](#)]
24. Shannon, R.D. Revised effective ionic radii and systematic studies of interatomic distances in halides and chalcogenides. *Acta Crystallogr. Sect. A* **1976**, *32*, 751–767. [[CrossRef](#)]
25. Ottonello, G.; Bokreta, M.; Sciuto, P.F. Parameterization of energy and interactions in garnets: End-member properties. *Am. Mineral.* **2015**, *81*, 429–447. [[CrossRef](#)]
26. Moore, R.K.; White, W.B.; Long, T.V. Vibrational spectra of the common silicates: I. The garnets. *Am. Mineral.* **1971**, *56*, 54–71.
27. Hofmeister, A.M.; Fagan, T.J.; Campbell, K.M. Single-crystal IR spectroscopy of pyrope-almandine garnets with minor amounts of Me and Ca. *Am. Mineral.* **1996**, *81*, 418–429. [[CrossRef](#)]